RSC Advances

PAPER

View Article Online
View Journal | View Issue

Cite this: *RSC Adv.*, 2024, **14**, 32328

A self-regulated shielding layer induced by an electrolyte additive for alkaline Al–air batteries

Lei Guo, *[ac] Yongbiao Huang,[b] Ida Ritacco,[d] Renhui Zhang,*[b] Jun Chang,[ae] Mohammad K. Al-Sadoon,[f] Peng Chen [a] and Amir Mahmoud Makin Adam[a]

Aqueous Al–air batteries (AABs) are considered promising electrochemical energy devices due to their high-energy density, high-capacity density, and stable discharge voltage. However, the self-corrosion, passivation, and parasitic hydrogen precipitation side reactions in the aqueous electrolyte degrade the performance of these batteries, limiting their development. To overcome the problems related to the use of AABs, we introduce ethylenediaminetetraacetic acid disodium salt (EDTA-2Na) as an additive to the alkaline electrolyte. EDTA-2Na adsorbs strongly to the Al anode interface creating a protective layer capable of inhibiting water-induced parasitic reactions. In fact, in the presence of the additive, the hydrogen evolution tests have shown that the hydrogen evolution rate decreased from 0.70 to 0.30 mL cm^{-2} min^{-1}. In addition, the electrochemical tests indicated an inhibition efficiency of 55%, the full-cell discharge tests suggested an increase in the specific capacity density of the battery from 943.6 to 2381.7 mA h g^{-1} and the anode utilization increased from 31.6% to 80.9%, greatly improving the performance of the battery. Surface characterization of the Al alloy surface was also carried out to investigate the adsorption of EDTA-2Na on it. This electrolyte modification strategy provides a promising option for modulating the anode/electrolyte interface chemistry to achieve high-performance AAB.

Received 3rd September 2024
Accepted 8th October 2024

DOI: 10.1039/d4ra06356b

rsc.li/rsc-advances

1. Introduction

Due to the over-consumption of traditional fossil energy sources and their non-renewable and environmentally damaging nature, there is an urgent demand for green, and clean energy storage sources to replace the traditional sources.[1,2] Metal–air batteries have received widespread attention for their high-energy density and high-capacity density as well as environmental friendliness.[3–5] Among them, AABs are distinguished by the abundance of Al resources and the superior theoretical specific capacity density of Al relative to other metals. They can be used as disposable batteries in emergency power, range extenders, and military applications.[6–8] Consequently, more investigation into the advancement of AABs is vital.

However, the development of AAB has many limitations.[9] During the discharge process, the Al anode immersed in the alkaline solution undergoes self-corrosion and passivation phenomena which, combined with the parasitic hydrogen precipitation side-reaction that occurs at the cathode, greatly reduce the efficiency of the Al anode utilization, limiting the specific capacity density of the AAB and it development.[10,11] To enhance the anode utilization and increase the specific capacity density of AAB, researchers have devised various approaches to mitigate passivation phenomena at the Al anode and hydrogen evolution reactions.[12,13] These approaches include the use of anode alloys,[14] electrolyte additives,[15] solid electrolytes,[16] non-aqueous electrolytes,[17] highly concentrated electrolytes,[18] dual-electrolyte,[19] and other conditioning methods. Anodic alloying has shown efficacy in mitigating metal corrosion and enhancing the performance of metal–air batteries;[20–22] nonetheless, it is characterized by complexity and high operational costs.[23] Since both hydrogen precipitation reaction and anode polarization occur at the interface between the electrolyte and the electrodes, and the electrolyte is an important component linking the cathode and anode through ion transport, it governs the electrochemical process of the battery.[24] Therefore, the selection of a suitable electrolyte system is the key to achieving high-performance AAB. Electrolyte additives are gaining widespread attention as an efficient, economical, and convenient method.

Adding additives to the electrolyte turns out to be a valid method to prevent the AAB corrosion during the discharge phase. Based on the composition of the substance, the additives can be classified into inorganic additives, organic additives, and

[a]School of Material and Chemical Engineering, Tongren University, Tongren 554300, China. E-mail: chygl@gztrc.edu.cn
[b]School of Materials Science and Engineering, East China Jiaotong University, Nanchang 330013, China. E-mail: 3067@ecjtu.edu.cn
[c]Jixian Research Center of Green Functional Materials, Linfen 042200, China
[d]Department of Chemistry and Biology, University of Salerno, Via Giovanni Paolo II, 132, 84084 Fisciano, Salerno, Italy
[e]Guizhou Provincial Key Laboratory for Cathode Materials of New Energy Battery, Tongren 554300, China
[f]Department of Zoology, College of Science, King Saud University, P.O. Box 2455, Riyadh 11451, Saudi Arabia

complex additives. Inorganic additives are commonly used in the electrolyte of AAB. Generally, inorganic additives contain elements with high hydrogen overpotentials (*e.g.*, Zn, Mg, Sn, Mn, Pb, and Bi) which, during the discharge process, react with the alkaline solution to form a layer of inorganic protective film can adsorb on the Al surface, thus reducing the corrosion of the Al anode, and at the same time, the hydrogen precipitation reactions on the Al surface.[25] In this way, the inorganic additive can effectively protect the Al surface and improve the performance of the AAB. For example, Choi *et al.* studied the inhibition effects of three kinds of inorganic additives, arsenic oxide, anhydrous monobasic sodium phosphate, and antimony trioxide in the AAB.[26] The results showed that the three kinds of inorganic additives can reduce the dissolution of Al and reduce the generation of hydrogen evolution reactions, confirming that the inorganic additives can improve the performance of the AAB. However, the protective film formed by the inorganic additives on the Al surface is not strong as it results in being loose and porous. For this reason, during the discharge process, the film is continuously dissolved by the electrolyte which then reduces its protective ability. Organic additives are expected to unravel some of the shortcomings of inorganic additives thanks to their unique molecular structure. Most organic additives contain in their structure polar heteroatoms, which usually have lone pairs of electrons (*e.g.*, O, N, S) able to interact with the orbitals of Al and to adsorb onto the Al surface through chemical bonding. The remaining organic additives generate protective layers by forming, for example, hydrogen bonds or other interactions. Especially with some long-chain organic additives, the polar portion adsorbs on the surface of Al and the non-polar portion extends into the solution, and this combination creates a stronger protective effect on the surface of Al. In this regard, Wu *et al.* introduced sucrose as an additive to the alkaline electrolyte of AAB.[27] They found that the sucrose molecules present in the alkaline electrolyte were able to reduce the number of active water molecules in the electrochemical environment, effectively inhibiting the self-corrosion reaction of the Al anode. Another example is Zhu *et al.* who studied the imprinting effect of two surfactants, betaine, and dodecyldimethyl betaine, in alkaline solution on AAB.[28] The results showed that the chemisorption of meso-hydrophilic groups and the interaction of long alkyl chains in the two surfactants might hinder the diffusion of OH^- and Al^{3+} ions along the Al alloy/solution interface, thus effectively slowing down the self-corrosion of the Al anode.

These green, low-cost organic additives can improve the performance of AAB without causing environmental damage.[29,30] Therefore, it is intriguing to examine these compounds as additions for alkaline AABs. In this study, we examined EDTA-2Na as an additive for alkaline AABs, characterized as a cost-effective and non-toxic organic compound. EDTA-2Na is also used as a chelating agent. When it dissolves in an alkaline solution, it splits into two parts: positively charged Na^+ and negatively charged EDTA. The negatively charged molecules have many carboxyl groups that can easily connect with the atomic orbitals of Al atoms to form a stable complex. This stable complex can act as a protective film on the Al surface and adsorb on the surface of the Al anode to reduce the corrosion of Al. Herein, we elucidated the inhibition mechanism of EDTA-2Na additive, which provides a new strategy for the electrolyte modification of AAB in the future.

2. Experimental

2.1. Materials and reagents

The combined internal composition of the metal anode rate used in this work was (Mg 2.18%, Si 0.06%, Zn 0.01%, Mn 0.06%, Cr 0.17%, Fe 0.19%, and the rest Al). NaOH was purchased from Shanghai Rhawn Chemical Co., Ltd and EDTA-2Na was purchased from Shandong Yusuo Chemical Technology Co. 4 M NaOH solution was prepared by dissolving NaOH powder in deionized water. All the experiments were carried out at room temperature (25 ± 1 °C), and three parallel experiments were performed for each group to ensure the accuracy of the experiments.

2.2. Hydrogen evolution experiments

The hydrogen evolution volume from Al alloys in 4 M NaOH solutions without and with different concentrations of ETDA-2Na was determined by the drainage method. A sample of Al alloy with an exposed area of 1 cm^2 was placed in a conical flask connected to a catheter. The total reaction time for each hydrogen evolution experiment was 30 min and the drainage was read every 5 min. The rate of hydrogen evolution (R_{H_2}) during the reaction cycle was calculated by the following equation:[10]

$$R_{H_2} = \frac{V}{A \times T} \quad (1)$$

where R_{H_2} indicates the hydrogen evolution rate, A denotes the area of the specimen (cm^2), V denotes the volume of hydrogen collected (mL), and T denotes the reaction time (min). Further, the corrosion inhibition efficiency (η_{H_2}) was calculated by the following equation:

$$\eta_{H_2}(\%) = \frac{R_0 - R_{inh}}{R_0} \times 100 \quad (2)$$

where R_0 and R_{inh} are the hydrogen evolution rates of sample in NaOH solution without and with ETDA-2Na, respectively.

2.3. Electrochemical measurements

Electrochemical measurements were accomplished in the laboratory at room temperature using a CHI760E electrochemical station. A conventional three-electrode system was used, in which the Hg/HgO electrode was used as the reference electrode, the platinum plate as the counter electrode, and the Al alloy as the working electrode. The Al electrode was free-corroded in 4 M NaOH solution for 30 min and the open circuit potential (OCP) was measured. AC impedance spectroscopy (EIS) measurements were performed at the E_{OCP} using an AC signal with an amplitude of 5 mV in the frequency range of 10 kHz to 1 Hz, and the obtained impedance data were analyzed by equivalent circuit modeling using ZsimpWin 3.6 software. Potentiodynamic polarization (PDP) tests were performed over a potential range of ±250 mV with respect to the E_{OCP} at a scan rate of 0.5 mV s^{-1}.

2.4. Surface characterization

Al alloy samples of 1 cm × 1 cm × 0.2 cm were immersed in 4 M NaOH solution at room temperature and treated for 1 h without and with the optimal concentration of ETDA-2Na additive, respectively. After treatment, the Al alloy samples were cleaned and dried. The surface morphology of the Al alloys after immersion was investigated using scanning electron microscopy (SEM, JEOL-JSM7800F) and atomic force microscopy (AFM, MFP-3D-BIO). Meanwhile, the absorbance of the electrolyte after discharge was detected using a UV-visible spectrophotometer (UV-vis, TU-1901). The bonding information between the Al alloy surface and the ETDA-2Na inhibitor was analyzed by X-ray photoelectron spectroscopy (XPS, Thermo Fisher Nexsa G2). The functional groups on the electrode surface was validated through attenuated total reflection Fourier transform infrared spectroscopy (ATR-FTIR, IRTracer-100). Finally, the water contact angle measurement was performed using a goniometer (CA, JY-PHa) to analyze the effect of the ETDA-2Na additive on the contact angle of the Al surface.

2.5. Al–air full battery test

Battery performance was tested with a homemade AAB device, which consists of an Al anode, a commercially available air cathode, and an electrolyte. The performance of the AAB was evaluated by inserting the electrolyte, with and without additions, into a plastic container and conducting a continuous flow of the electrolyte using a circulation pump. A cyclic intermittent constant-current discharge test was conducted at a current density of 20 mA cm^{-2} for 1 hour. Subsequently, the system was maintained at open circuit potential (OCP) for 20 minutes, repeating this cycle for a total of four rounds. Polarization curves and power density curves were acquired using linear scanning voltammetry (LSV) at a scan rate of 1 mV s^{-1}. The formulas for battery anode utilization (U_a), capacity density (Q), and energy density (W) are as follows:[31,32]

$$U_a = \frac{9It}{\Delta mF} \times 100\% \quad (3)$$

$$Q = \frac{It}{\Delta m} \quad (4)$$

$$W = \frac{EIt}{\Delta m} \quad (5)$$

where I denotes the discharge current (mA), t represents discharge time (h), Δm denotes weight loss of Al, F represents the Faraday constant (C mol^{-1}), and E denotes the average discharge (V).

3. Results and discussion

3.1. Hydrogen evolution test

The drainage device is illustrated in Fig. 1a. The amount of hydrogen generated by the Al alloy in a 4 M NaOH solution with varying EDTA-2a additive quantities is shown in Fig. 1b. The results indicate that the volume of hydrogen produced is reduced when EDTA-2Na is added to the solution, in particular, the Al alloy releases the least volume when 7 mM of additive is present in NaOH solution. Fig. 1c shows the hydrogen evolution rate and corrosion inhibition efficiency. The addition of EDTA-2Na causes a decrease of the hydrogen evolution rate on the Al alloy from 0.70 to 0.30 mL cm^{-2} min^{-1} when 7 mM of EDTA-2Na is added to the NaOH electrolyte. In the same conditions, the inhibition efficiency reaches 57%. The hydrogen evolution rate is related to the number of hydrogen electrolyte sites on the Al surface.[33] Most likely the adsorption of EDTA-2Na on the surface of Al decreases the hydrogen evolution active sites on the Al surface, thus reducing the generation of the hydrogen evolution reactions and lowering the hydrogen precipitation rate. This indicates that EDTA-2Na has a great inhibitory effect on the hydrogen evolution corrosion of the concerned Al alloy.

3.2. Open circuit potential and polarization curves

Fig. 2a shows the open-circuit variation curves of the Al alloy in 4 M NaOH without and with different concentrations of EDTA-2Na additive. All curves have the same trend, that is an initial increase until reaching the potential plateau. The initial positive voltage shift occurs due to anodic polarization generated by the formation of insoluble oxides and hydroxides, but the voltage stabilizes over time. The open-circuit voltage decreased with the addition of EDTA-2Na. This may be attributable to the suppression of the hydrogen evolution process. The corrosion process involves a multi-step dissolution of Al at the anode and

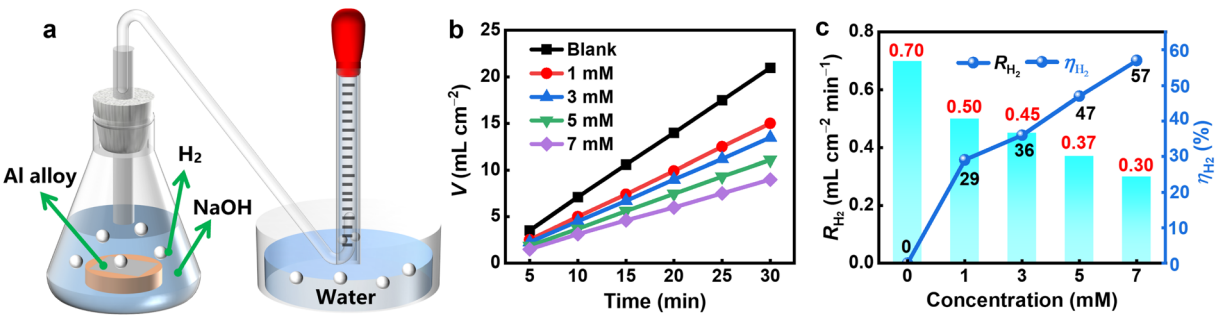

Fig. 1 (a) Diagram of hydrogen evolution test device, (b) hydrogen evolution volume, and (c) hydrogen evolution rate of Al alloy in NaOH solutions containing different concentrations of EDTA-2Na.

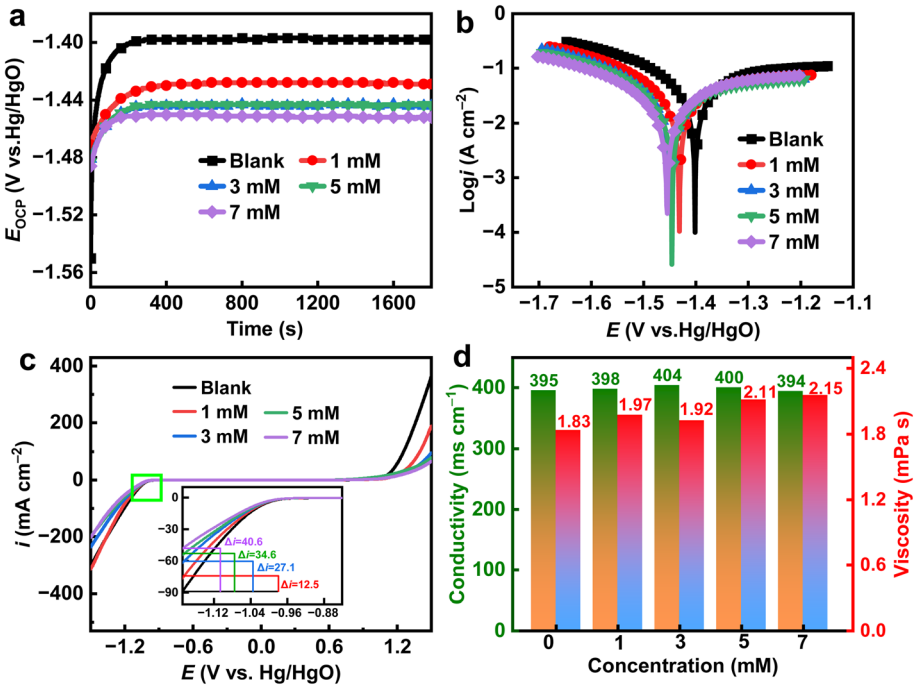

Fig. 2 (a) OCP curves, (b) PDP curves, (c) electrochemical stability windows, and (d) conductivity and viscosity of different electrolytes.

a parasitic hydrogen evolution reaction at the cathode. The reaction process is shown below:

Multi-step Al dissolution process:[34,35]

$$Al + OH^- \rightarrow Al(OH)_{1,ads} + e^- \quad (6)$$

$$Al(OH)_{1,ads} + OH^- \rightarrow Al(OH)_{2,ads} + e^- \quad (7)$$

$$Al(OH)_{2,ads} + OH^- \rightarrow Al(OH)_{3,ads} + e^- \quad (8)$$

$$Al(OH)_{3,ads} + OH^- \rightarrow Al(OH)_{4,ads}- \quad (9)$$

$$Al(OH)_{4,ads}{}^- \rightarrow Al(OH)_3 + OH^- \quad (10)$$

Parasitic hydrogen evolution process:[36]

$$H_2O + e^- \rightarrow H_{ads} + OH^- \quad (11)$$

$$H_{ads} + H_2O + e^- \rightarrow H_2 + OH^- \quad (12)$$

The use of EDTA-2Na prevents the Al alloy from direct exposure to water in the electrolyte. It diminishes the hydrogen evolution sites on the surface of the Al alloy, hence mitigating corrosion.

Fig. 2b shows the polarization curves of Al alloy by using different electrolytes. With the introduction of EDTA-2Na, both anodic and cathodic branches of the polarization curves shift towards the low current density region, which indicates that EDTA-2Na is a hybrid additive. The results related to the OCP curves and the polarization curves suggest a reduction in the anode polarization deriving from a reduction in the hydrogen evolution sites. These sites decrease due to the adsorption of the EDTA-2Na on the anode which interacts with the Al surface through its carboxyl groups. The corrosion potential (E_{corr}), corrosion current density (i_{corr}), cathodic and anodic slopes (β_c/β_a) were calculated using the Tafel extrapolation, and the relevant information is reported in Table 1. The corrosion inhibition efficiency (η_{PDP}) and the corrosion rate (CR) were computed with the following formula:[37,38]

$$\eta_{PDP}(\%) = \frac{i_{corr} - i_{corr(inh)}}{i_{corr}} \times 100 \quad (13)$$

$$CR = \frac{3.28M}{nd} \times i_{corr} \quad (14)$$

where i_{corr} and $i_{corr(inh)}$ are the corrosion current density for Al anode in 4 M NaOH solution without and with EDTA-2Na,

Table 1 Polarization parameters for Al anode in 4 M NaOH electrolyte with and without various concentrations of EDTA-2Na

C (mM)	E_{corr} (V)	β_a (mV dec^{-1})	$-\beta_c$ (mV dec^{-1})	i_{corr} (mA cm^{-2})	CR (mm per year)	η_{PDP} (%)
Blank	−1.397	314.4	203.9	56.92	621.5	—
1	−1.428	340.6	190.7	39.82	434.8	30.0
3	−1.443	342.8	192.8	33.89	370.0	40.4
5	−1.442	318.3	189.3	30.71	335.3	46.0
7	−1.452	252.9	193.3	25.69	280.5	54.9

respectively. M is atomic mass, n is the number of electrons freed by the corrosion reaction, and d is density.

The results reported in Table 1 showed once again the hybrid corrosion inhibitor nature of EDTA-2Na. The addition of the additive to the electrolyte caused a decrease in the cathodic slope and anodic slope.[39,40] At 7 mM EDTA-2Na, the density of the current decreased from 56.92 mA cm^{-2} to 25.69 mA cm^{-2} in the blank, and η_{PDP} reached 54.9%. The CR value of the introduced addition gets smaller, indicating that EDTA-2Na effectively mitigated the corrosion of Al. Fig. 2c shows the electrochemical stabilization windows without and with different concentrations of EDTA-2Na. It can be seen that the electrochemical stability window gradually increases with the increase of EDTA-2Na concentration. The reduction current (hydrogen evolution) density changes by 40.6 mA cm^{-2}, going from −88.78 mA cm^{-2} for the pristine 4 M NaOH to −48.18 mA cm^{-2} for the solution with 7 mM EDTA-2Na. This variation indicates that the Al electrode is stabilized in a larger potential range as the additive concentration increases. After the adsorption of EDTA-2Na, only a small number of water molecules are involved in the parasitic self-corrosion process.[41,42] The conductivity and viscosity of the electrolyte under different conditions were also tested. From Fig. 2d, the addition of EDTA-2Na to the electrolyte caused a stable change in the conductivity and a slight increase in the viscosity. This indicates that the introduction of EDTA-2Na does not affect the conductivity of the electrolyte but affects the hydrogen bond network forming in the solution.[43]

3.3. EIS measurements

Fig. 3 shows the Nyquist and Bode plots of the Al alloy under different concentrations of EDTA-2Na in the 4 M NaOH electrolyte. As shown in Fig. 3a, all the Nyquist plots have the same trend and are composed of three components, that is the low-frequency capacitive loop, the mid-range induced arc, and the high-frequency capacitive loop, respectively. The initial capacitive loop in the high-frequency region is attributed to the loss of an electron, hence the oxidation of Al to Al^+. This is the rate-determining step of the Al dissolution.[34] An inductive loop appears at mid-frequency, indicating the adsorption of the additive EDTA-2Na and the accumulation of intermediates such as $Al(OH)_{1-4,ads}$, OH^- and H_2 on the Al surface together.[35] The second capacitive loop in the low-frequency region is associated with the oxidation of Al to Al^{3+}, which is considered to be a fast complementary step.[44] With the addition of EDTA-2Na, the radii of the impedance loops both increased. This indicates an increase of the electrolyte polarization resistance and a decrease of the corrosion rate. The corresponding Bode amplitude and phase angle plots are shown in Fig. 3b and can be used to describe the nature of the purely capacitive behaviors.[45] The modulus *versus* log(frequency) graphs indicate that the absolute $|Z|$ impedance values for the examined alloy in the inhibited solution are much higher than that in the pristine NaOH solution. Two time constants are identified, corresponding to the electron charge transfer process across the double layers, from the interface layer in the high-frequency region to the corrosion product layer in the low-frequency range.

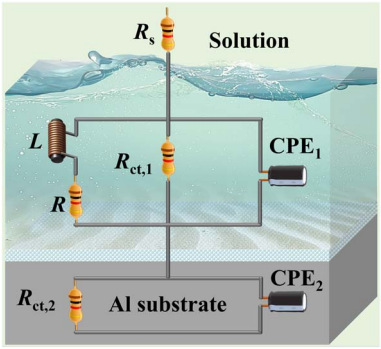

Fig. 4 The equivalent circuit used for fitting the EIS data.

The equivalent circuit diagram as shown in Fig. 4 was used for further analysis of the EIS data. Herein, R_s is the solution resistance, the high-frequency region of the equivalent circuit consists of a constant phase element (CPE$_1$) and a charge transfer resistor ($R_{ct,1}$). The mid-frequency region consists of inductance (L) and resistance (R), and the low-frequency region consists of a constant phase angle element (CPE$_2$) and a charge transfer resistor ($R_{ct,2}$). Polarization resistance (R_p) and corrosion inhibition efficiency (η_{EIS}) are described below:[46]

$$R_P = \frac{R_{ct,1} \times R}{R_{ct,1} + R} + R_{ct,2} \quad (15)$$

$$\eta_{EIS}(\%) = \frac{R_P - R_P^0}{R_P^0} \times 100 \quad (16)$$

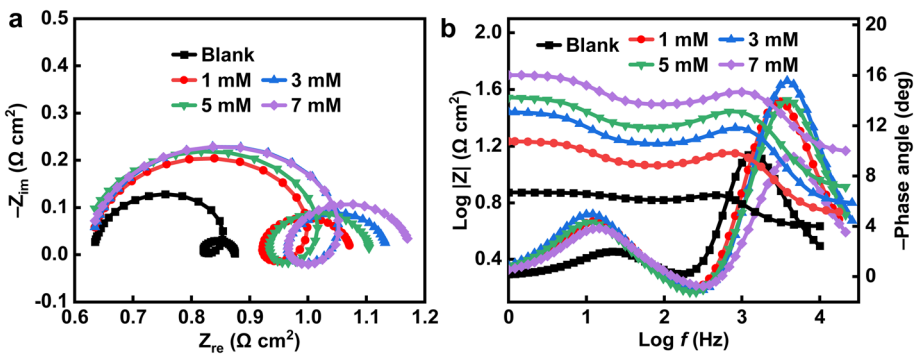

Fig. 3 (a) Nyquist and (b) Bode plots of Al alloy in 4 M NaOH electrolyte with different concentrations of EDTA-2Na.

Table 2 EIS parameters of Al alloy in 4 M NaOH without and with EDTA-2Na additive

		CPE$_1$					CPE$_2$				
C (mM)	R_s (Ω cm^2)	Y_0 (10^{-4} S s^n cm^{-2})	n_1	$R_{ct,1}$ (Ω cm^2)	L (10^{-5} H cm^2)	R (Ω cm^2)	Y_0 (10^{-1} S s^n cm^{-2})	n_2	$R_{ct,2}$ (Ω cm^2)	R_p (Ω cm^2)	η_{EIS} (%)
Blank	0.632	5.855	1.000	0.180	3.064	0.082	1.146	1.000	0.123	0.179	—
1	0.725	1.502	1.000	0.328	5.398	0.130	0.712	1.000	0.151	0.234	23.4
3	0.564	1.845	1.000	0.288	4.187	0.123	0.842	0.992	0.160	0.246	27.2
5	0.838	1.548	1.000	0.312	4.728	0.127	0.692	1.000	0.181	0.271	33.9
7	1.152	1.001	1.000	0.333	4.044	0.125	5.434	1.000	0.270	0.371	51.7

wherein, R_p and R_p^0 are the polarization resistance with and without EDTA-2Na, respectively. Table 2 specifically demonstrates the electrochemical parameters associated with EIS. When the EDTA-2Na concentration is 7 mM, the R_p value reaches 0.371 Ω cm^2, and the corresponding η_{EIS} is 51.7%.

The rise in the R_p value signifies an augmentation in the resistance at the interface between the electrode and the electrolyte, implying that EDTA-2Na may adsorb onto the surface of the Al anode to create a shielding layer.

3.4. Surface morphology analysis

To enhance the observation of corrosion in Al alloys under various situations and to ascertain if the incorporation of EDTA-2Na mitigated the corrosion of Al alloys. We conducted surface characterisation of Al alloys under three distinct situations using both SEM and atomic force AFM techniques. Fig. 5 displays the surface characterization findings for the bare metal matrix (sanding alone), the blank (containing just 4 M NaOH solution), and the Al alloy that was exposed to 4 M NaOH solution containing 7 mM EDTA-2Na. Fig. 5a shows the SEM findings of a pure substrate. In this situation, the Al surface is smooth with polished scratches. The SEM results of Al alloy under blank conditions were given in Fig. 5b. Here, the Al surface has severe corrosion, and the surface has fractured. Fig. 5c displays the SEM findings of an Al alloy that includes 7 mM EDTA-2Na in an alkaline solution. It is evident that the addition of the additive reduces the surface cracks of the Al alloy and makes the surface smoother. These findings align with the AFM data shown in Fig. 5d (pure matrix), 5e (blank), and 5f (including additives), which indicated surface roughness values of 74.8, 201, and 149 nm, respectively.

In addition, we also carried out a water contact test on the surface of the soaked Al alloy to investigate the wetness of the Al surface. The observed contact angles were 39.2°, 33.8°, and 66.2°, respectively. The introduction of EDTA-2Na additive increased the contact angle, indicating that the corrosion reaction was reduced due to the existence of multiple hydrophobic carboxyl groups of EDTA-2Na.[47] The adsorption of EDTA-2Na on the Al surface covers some active sites. This procedure efficiently decreases the contact area between water molecules and Al and enhances the hydrophobic barrier of the surface. Thus, the incidence of self-corrosion in Al alloy can be minimized.

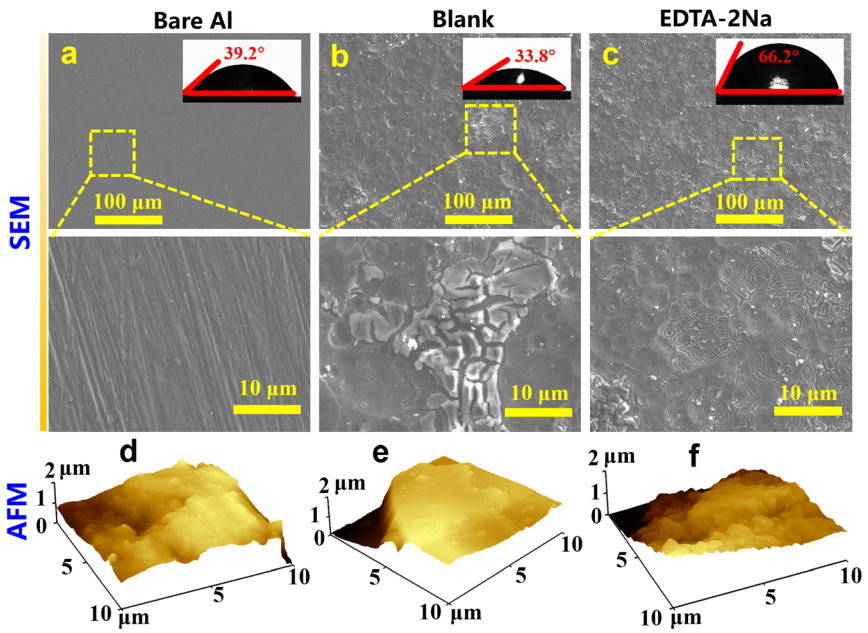

Fig. 5 SEM, CAM, AFM results of the Al alloy surface under different conditions.

3.5. Bonding configuration analysis

To comprehend the primary chemical composition of the shielding layer on the surface of the Al alloy after the incorporation of EDTA-2Na, the Al alloy surface was examined using ATR-FTIR and XPS methodologies. The ATR-FTIR spectra of a variety of samples are illustrated in Fig. 6a, which reveals bonding information. The peaks are barely discernible on the bare Al surface as a result of its non-reactive nature toward other substances. The EDTA-2Na powder has prominent peaks at 3521 cm^{-1} and 899 cm^{-1}, which correspond to the N–H and C–N bonds, respectively. The FTIR spectra of Al after being immersed in the solution containing the additive also indicate the existence of N–H and C–N groups on the substrate surface. These groups exhibit peak shifts that are somewhat different from those of the untreated sample.[48] A obviously peak at 712 cm^{-1} indicates the presence of a chemical bond between Al and oxygen on the anode surface.[49]

Fig. 6b displays the survey XPS evidence of the Al surface after immersion in a 4 M NaOH solution containing 7 mM EDTA-2Na for one hour. The O 1s mainly consists of C=O bond at 533.3 eV, C–O bond at 532.3 eV, and O–H bond at 531.4 eV (Fig. 6c).[50] The Al 2p peaks with energy levels of 76.8 eV, 75.7 eV, and 74.1 eV correspond to Al, Al_2O_3, and $Al(OH)_3$, respectively (Fig. 6d).[51] The C 1s peaks were seen at certain energy levels: 290.8 eV for the O=C–O bond, 287.1 eV for the C–N bond, and 284.8 eV for the C=C bond (Fig. 6e).[52] The peak of N 1s appeared at 401.4 eV which can be ascribed to the N–H bond (Fig. 6f).[53] The presence of the N–H bond and the C–N bond indicates that EDTA-2Na can be adsorbed on the surface forming a protective barrier that reduces the corrosion of the Al alloy.

3.6. Electrochemical performances of AAB

Initially, we conducted a theoretical investigation of the impact of the battery lugs' position. The COMSOL program was used to model the lug in three positions: side, off-central, and central. The Al anode's surface potential and current density distributions are illustrated in Fig. 7. The potentials at the three electrode lugs are more negative. The examination of the current density distribution on the electrode surface shows a very uniform distribution of current particularly at the central location. One may infer that the consumption of Al alloy remains more constant throughout the battery response in comparison to the consumption at the side and off-central locations. This may somewhat enhance the longevity of the Al alloy anode and prevent the poor utilization of the anode resulting from the separation and breakage of Al residue after uneven corrosion.[54]

In light of the aforementioned results, we conducted battery testing by constructing a bespoke AAB with center lugs (Fig. 8a). The homemade Al–air battery comprises an Al anode, an air cathode, and an electrolyte. The air electrode has a thickness of 0.5 mm and comprises manganese dioxide, activated carbon, and conductive carbon black, organized into three layers: a catalytic layer, a current collecting layer, and a waterproof dispersion layer. Among them, high-purity nickel mesh was

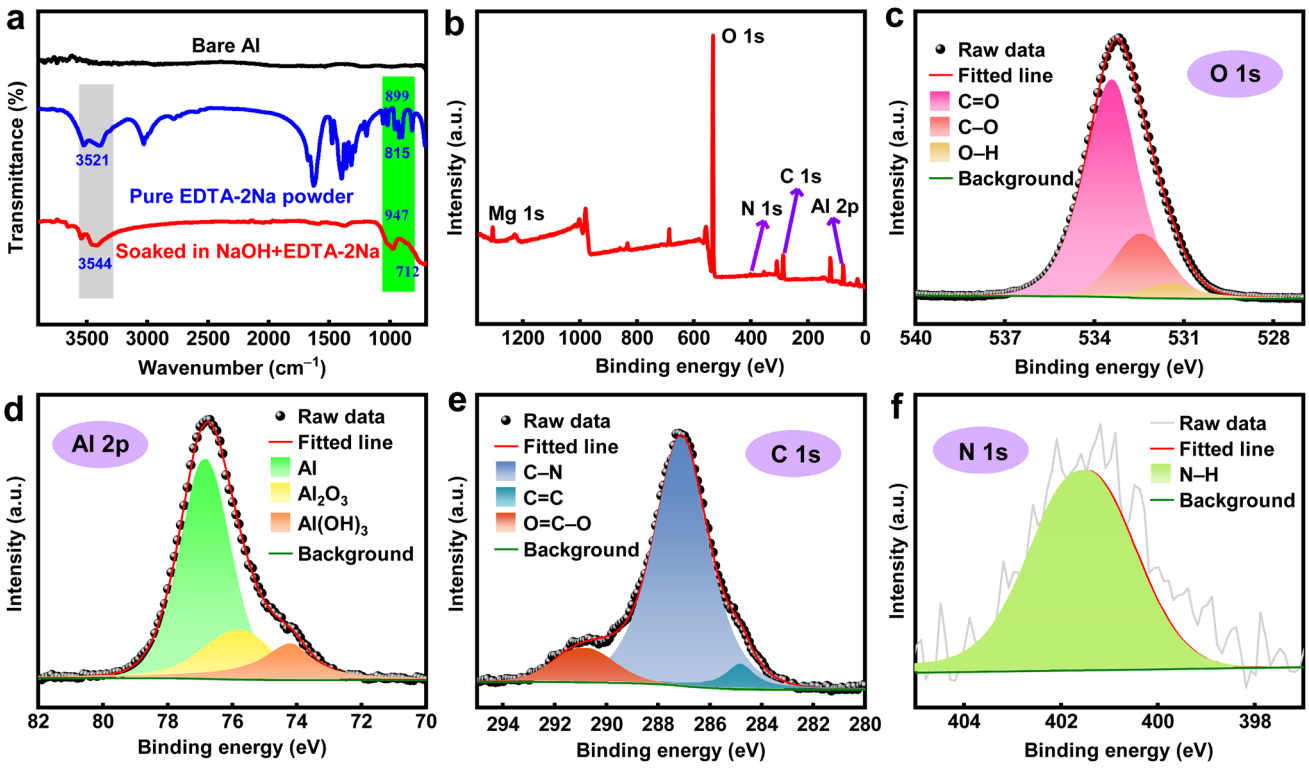

Fig. 6 (a) ATR-FTIR and XPS analysis of Al surface after immersion in 4 M NaOH with 7 mM EDTA-2Na, (b) survey XPS spectra, (c) O 1s, (d) Al 2p, (e) C 1s, and (f) N 1s.

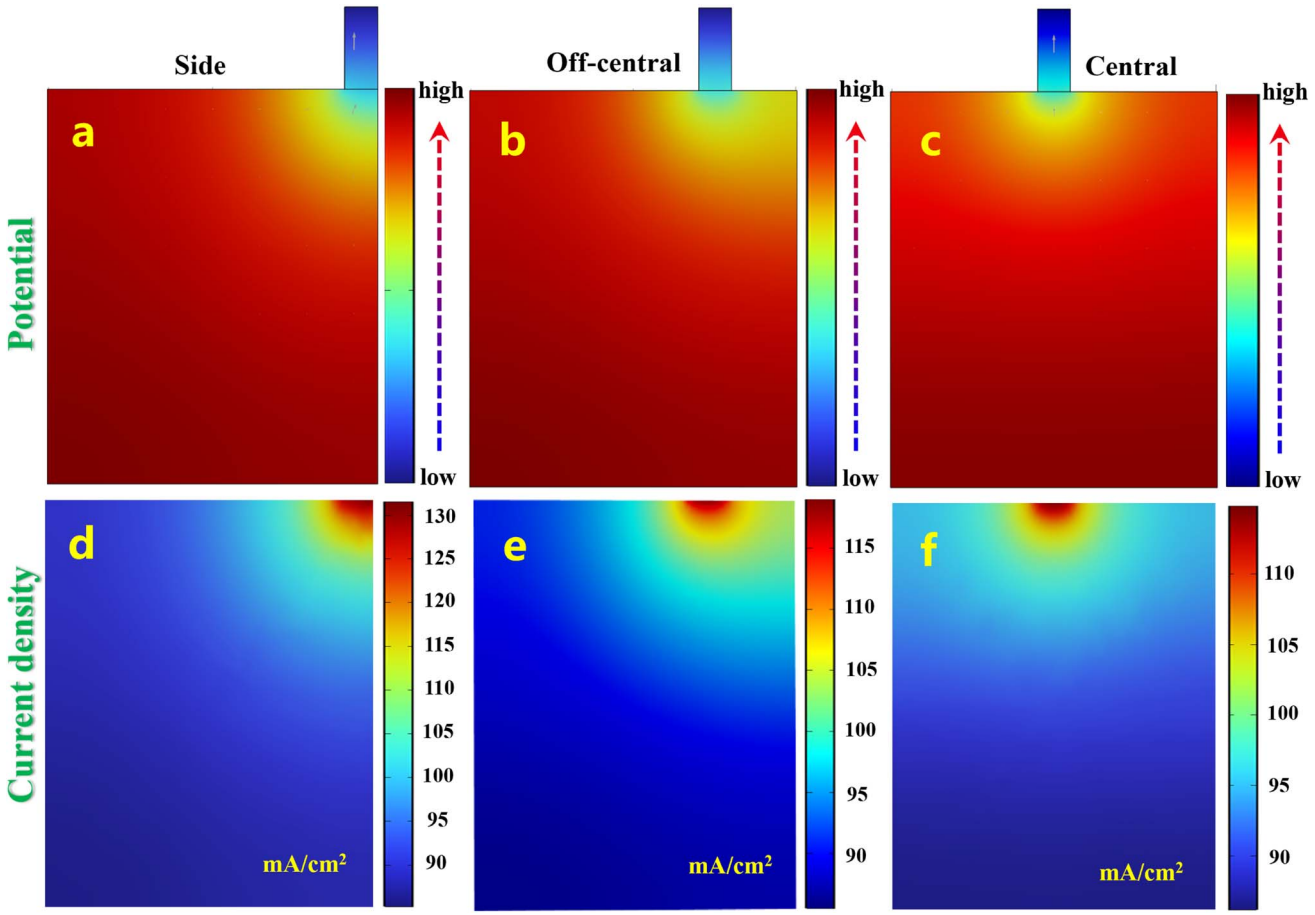

Fig. 7 (a–c) Potential and (d–f) current density distributions on the surface of Al anode with varying lug locations.

used as the collection carrier. The electrolyte (100 mL) containing EDTA-2Na and without EDTA-2Na was poured into a plastic bottle and circulated by a pump during the evaluation of the prepared cell. According to the data shown in Fig. 8b, the battery's capacity density rose from 943.6 to 2381.7 mA h g^{-1} after being discharged at a current density of 20 mA cm^{-2} for one hour. Intermittent discharge experiments were implemented to replicate the practical applicability of the battery. The AAB with EDTA-2Na exhibited a more stable and elevated discharge voltage, as illustrated in Fig. 8c. Multi-step current discharge tests at different current densities were also carried out to evaluate the stability of the AAB. Current densities ranging from 1 to 120 mA cm^{-2} was applied for 10 minutes. The findings shown in Fig. 8d indicate that the discharge voltage produced with additives is greater than that of the blank when the current density is identical. The parameters associated with blank and additive-containing AAB are illustrated in Fig. 8g. Furthermore, Table 3 presents a thorough overview of the prior research conducted on various electrolyte additions for AAB. The data demonstrates that the EDTA-2Na has superior specific capacity and anode utilization in comparison to other additives.[28,55,56]

It is widely accepted that the polarization process is related to the power density of the battery.[39] Fig. 8e demonstrates that AAB with EDTA-2Na additive enhance their maximum power density and short-circuit current density from 28.5 mW cm^{-2}, 98.4 mA cm^{-2}, to 59.4 mW cm^{-2} and 137.4 mA cm^{-2}, respectively. To determine whether EDTA-2Na may be adsorbed on the surface of the Al when the AAB are discharged, the electrolyte was studied before and after galvanostatic discharge using UV-visible spectroscopy, as shown in Fig. 8f. The reduction in the magnitude of the absorbance peak upon discharge suggests a simultaneous reduction in the concentration of EDTA-2Na in the electrolyte, therefore indirectly confirming the adsorption of EDTA-2Na on the surface of Al.[57] The thermal imaging results indicate that the battery system experiences negligible temperature fluctuations during discharge, with a maximum recorded temperature of 32.1 °C (Fig. 8h). Thermal imaging results show negligible temperature fluctuations throughout the battery system during discharge, with a maximum recorded temperature of 32.1 °C (Fig. 8h). Additionally, the home-made AAB successfully operated a thermohydrometer (Fig. 8i).

3.7. Analysis of mechanism

As seen in Fig. 9a, the pristine solution exhibits a substantial concentration of hydroxyl ions. Once this stage is reached, an oxidation process takes place on the anode, resulting in the corrosion of the surface of the Al anode. Concurrently, the water

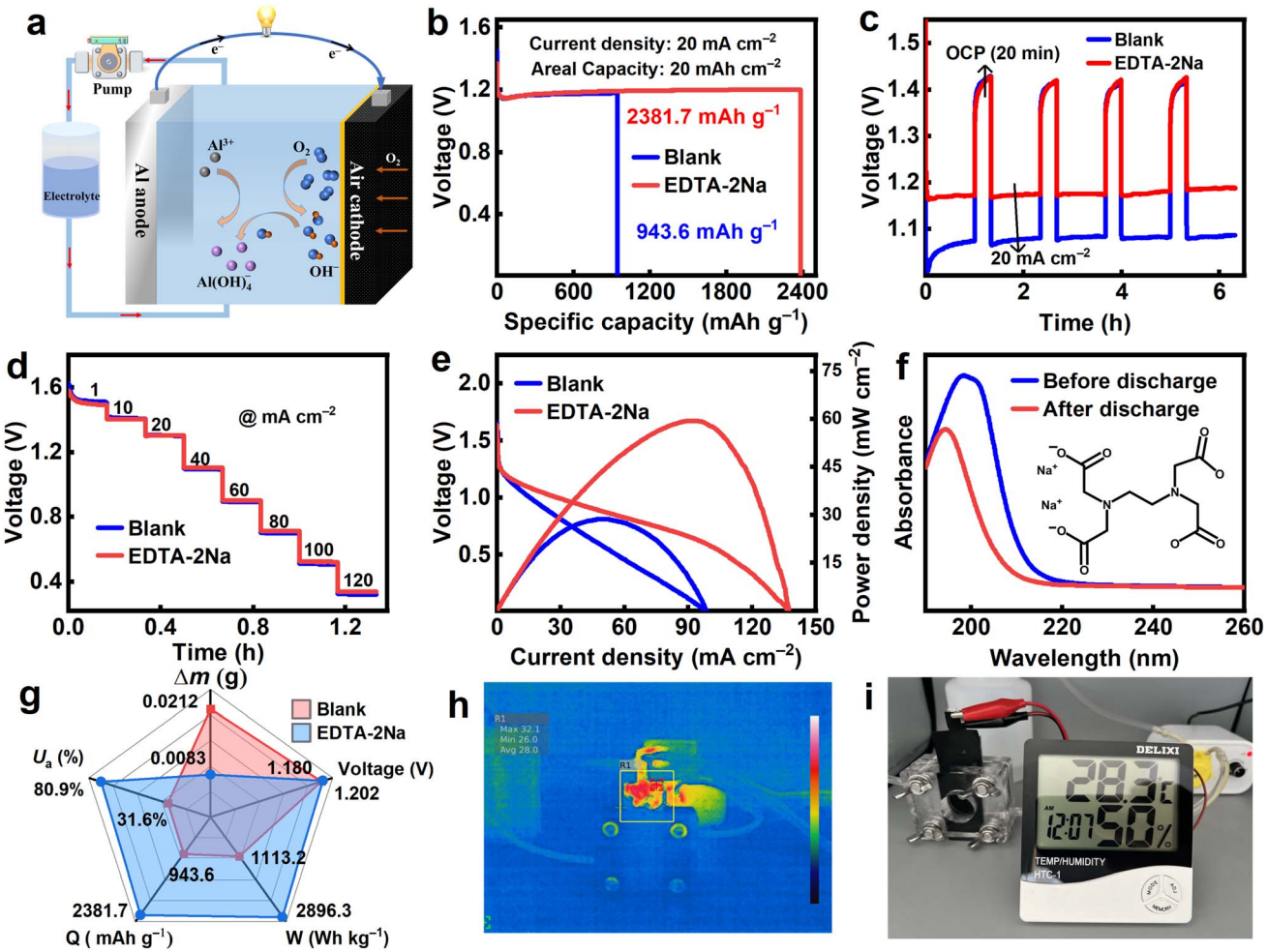

Fig. 8 (a) Schematic diagram of AAB device, (b) specific capacity curves, (c) intermittent discharge results, (d) multi-step current discharge curves, (e) polarization and power density curves, (f) UV-vis spectra of the regulated electrolyte before and after discharge, (g) comparison of battery parameters, (h) infrared thermographic image, (i) photographs of AAB powering an electronic device.

Table 3 Comparison of various electrolyte additives based on the consumed mass of Al anode materials

Additive	Al metal	Electrolytes	U_a (%)	Q (mA h g^{-1})	Ref.
EDTA-2Na	Al alloy	4 M NaOH	31.6	943.6	This work
		4 M NaOH + 7 mM EDTA-2Na	80.9	2381.7	
$CeCl_3$	Pure Al	4 M KOH	43.8	1294	*J. Electrochem. Soc.*[55]
		4 M KOH + 1.0 wt% $CeCl_3$	67.8	2000	
BS & BS-12	AA5052	4 M NaOH	42.1	1253.9	*J. Power Sources*[28]
		4 M NaOH + 1 mM BS	47.1	1403.5	
		4 M NaOH + 1 mM BS-12	49.2	1465.2	
AHMP + ZnO	Al-6061	4 M KOH	29.5	879	*Chem. Eng. J.*[56]
		4 M KOH + 4 mM ZnO	35.1	1044	
		4 M KOH + 10 mM AHMP	40.4	1203	
		4 M KOH + 4 mM ZnO + 10 mM AHMP	60.0	1785	

molecules engage in a reduction process on the Al surface, resulting in the production of hydrogen.[58] The presence of this parasitic hydrogen evolution process decreases the efficiency of the Al anode and simultaneously poses safety hazards for the use of AAB. The addition of EDTA-2Na to the 4 M NaOH solution, as seen in Fig. 9b, results in the coordination of Al atoms by multiple carboxyl groups in EDTA-2Na. This coordination leads to the adsorption of the additive on the Al surface and the formation of a shielding layer on the Al anode. This protective film inhibits the interaction of water in electrolyte with the Al surface while allowing the migration of OH^- unimpeded.[59] By decreasing the hydrogen evolution process, this improves the

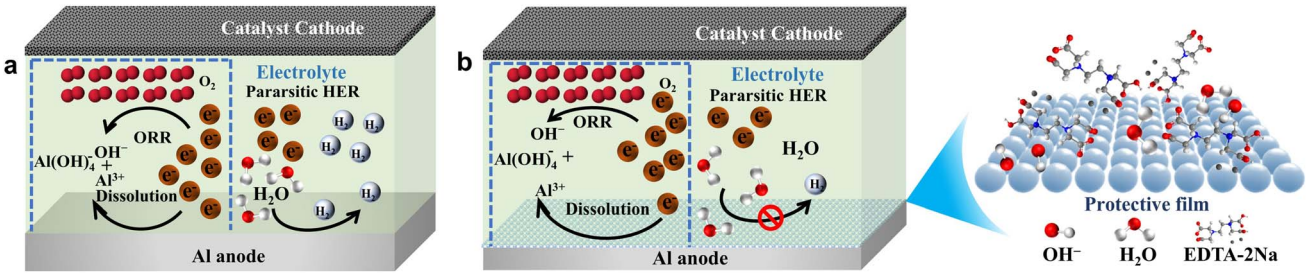

Fig. 9 Proposed mechanism of electrochemical behavior of Al alloy in (a) pristine and (b) inhibited electrolytes.

use of the Al anode and raises the battery's specific capacity without lowering the AAB's discharge efficiency.

4. Conclusion

The findings of this study demonstrate that EDTA-2Na is a very effective addition in alkaline AAB. The electrochemical results demonstrate a obviously decrease in the corrosion current density subsequent to the incorporation of EDTA-2Na into the electrolyte. This observation implies that the corrosion on the surface of the Al anode is diminished, consistent with the findings obtained from the hydrogen evolution experiments. Diverse characterization methods have further shown that the carboxyl groups of EDTA-2Na may interact with Al atoms, resulting in self-regulated adsorption on the surface of the Al anode and the formation of a shielding layer that prevents direct contact between water and Al in the solution. The full-cell experiment findings indicated that including EDTA-2Na into the NaOH solution enhanced anode utilization, elevated specific capacity density and energy density of the battery, hence augmenting its electrochemical performance. This pertains to the ability of EDTA-2Na to adsorb onto the surface of the Al anode, therefore creating a shielding barrier. The electrolyte regulation strategy proposed in this work is anticipated to facilitate the further development of AAB energy storage technology and establish a scientific foundation for developing high-performance AAB.

Data availability

Data will be made available on request.

Conflicts of interest

The authors declare that they have no known competing financial interests or personal relationships that could have appeared to influence the work reported in this paper.

Acknowledgements

We extend our appreciation to the Researchers Supporting Project number (RSP2024R410), King Saud University, Riyadh, Saudi Arabia. This work was supported by the National Natural Science Foundation of China (No. 22062022), the Foundation of the Department of Science and Technology of the Guizhou Province (No. QKHZDSYS[2023]006, QKHJCZK[2022]555, and QKHPTRC[2021]5643), the Project of Tongren Science and Technology Bureau (No. [2024]15), the Jiangxi Graduate Foundation of China (No. YC2022-s502), and the Foundation of Guizhou Key Laboratory of Green Metallurgy and Process Strengthening (No. QJJ[2023]026).

References

1 X. Luo, C. Ci, C. Zhou, J. Li, W. Xiong, Z.-H. Xie, M. Guo, D. Wu, B. Chen and Y. Liu, *Int. J. Biol. Macromol.*, 2023, **242**, 124712.
2 Y. Ma, K. Li, C. Li, X. Miao, T. Araki and M. Wu, *J. Power Sources*, 2024, **594**, 233999.
3 Y. Z. Shen, Y. Wang, Y. C. Li and Y. Liang, *Int. J. Electrochem. Sci.*, 2024, **19**, 100458.
4 M. Skonieczny, N. Izdebska, M. Królikowska and M. Marczewski, *Electrochim. Acta*, 2024, **500**, 144770.
5 S. Srivastava, D. Ahuja and P. K. Varshney, *J. Energy Storage*, 2024, **76**, 109588.
6 W. C. Tan, L. H. Saw, M. C. Yew, H. S. Thiam and K. Pei-Yu, *Chem. Eng. J.*, 2024, **488**, 151106.
7 Y. Tong, Y. Liu, Z. Gao, Z. Li, J. Zhang, Z. Qin, Y. Tang, Y. Xu, Y. Liu, Z. Wu and W. Hu, *J. Power Sources*, 2024, **606**, 234558.
8 Y. Yang, R. Zhao and Y. P. Chen, *RSC Adv.*, 2024, **14**, 23902–23909.
9 T. Dutta and J. Mary Gladis, *J. Energy Storage*, 2024, **86**, 111287.
10 Y. Nie, J. Gao, E. Wang, L. Jiang, L. An and X. Wang, *Electrochim. Acta*, 2017, **248**, 478–485.
11 K. Shahzad and I. I. Cheema, *J. Energy Storage*, 2024, **90**, 111795.
12 Y. Tian, W. Liu, T. Liu, X. Feng, W. Duan, W. Yu, H. Li, N. Deng and W. Kang, *J. Energy Chem.*, 2024, **98**, 244–261.
13 W. Wang, T. Yu, Y. Cheng, X. Lei, B. Wang, R. Guo, X. Liu, J. You, X. Wang and H. Zhang, *Nano Energy*, 2024, **125**, 109550.
14 F. Yu, Z. Liu, R. Zhao, J. Yang, J. Qiao and W. Hu, *J. Mater. Res. Technol.*, 2023, **27**, 4908–4919.
15 A. Kumar, L. Sharma and A. Verma, *J. Energy Storage*, 2024, **98**, 113039.
16 P. Meng, Z. Yang, M. Jiang, T. Zhao, J. Zhang and C. Fu, *Energy Storage Mater.*, 2024, **71**, 103663.
17 R. Revel, T. Audichon and S. Gonzalez, *J. Power Sources*, 2014, **272**, 415–421.

18 S. Wu, S. Hu, Q. Zhang, D. Sun, P. Wu, Y. Tang and H. Wang, *Energy Storage Mater.*, 2020, **31**, 310–317.
19 P. Teabnamang, W. Kao-ian, M. T. Nguyen, T. Yonezawa, R. Cheacharoen and S. Kheawhom, *Energies*, 2020, **13**, 2275.
20 J. Liu, H. Hu, T. Wu, J. Chen, X. Yang, N. Wang and Z. Shi, *J. Magnesium Alloys*, 2024, **12**, 1554–1565.
21 N. Wang, J. Liang, J. Liu, Q. Cai, J. Li, J. Chen, T. Huang and Z. Shi, *J. Power Sources*, 2022, **517**, 230707.
22 W. Zhang, B. Feng, L. Huang, Y. Liang, J. Chen, X. Li, Z. Shi and N. Wang, *Appl. Catal. B: Environ. Energy*, 2024, **358**, 124450.
23 R. Buckingham, T. Asset and P. Atanassov, *J. Power Sources*, 2021, **498**, 229762.
24 Y. Sun, J. Zhang, T. Huang and A. Yu, *Electrochem. Commun.*, 2024, **163**, 107726.
25 W. C. Tan, L. H. Saw, M. C. Yew, H. S. Thiam and K. Pei-Yu, *Chem. Eng. J.*, 2024, **488**, 151106.
26 S. R. Choi, S. J. Song and J. G. Kim, *Int. J. Electrochem. Sci.*, 2020, **15**, 8928–8942.
27 P. Wu, Q. Zhao, H. Yu, Z. Tang, Y. Li, D. Huang, D. Sun, H. Wang and Y. Tang, *Chem. Eng. J.*, 2022, **438**, 135538.
28 Y. Zhu, X. Li, D. Zhang and L. Gao, *J. Power Sources*, 2021, **515**, 230646.
29 S. Islam, S. M. A. Nayem, A. Anjum, S. Shaheen Shah, A. J. S. Ahammad and M. A. Aziz, *Chem. Rec.*, 2024, **24**, e202300017.
30 H. Wen, Z. Liu, J. Qiao, R. Chen, G. Qiao and J. Yang, *Int. J. Energy Res.*, 2020, **44**, 10652–10661.
31 B. Rani, J. K. Yadav, P. Saini, A. P. Pandey and A. Dixit, *RSC Adv.*, 2024, **14**, 17628.
32 H. Wang, J. Wang, Z. Jin, H. Li, H. Dou, J. Shi, C. Wei and Q. Gao, *J. Power Sources*, 2023, **566**, 232920.
33 S. Kumar, R. Kumar, N. Goyal, A. Yadav, S. Bm and B. Sahoo, *ACS Appl. Nano Mater.*, 2024, **7**, 16422–16437.
34 H. Cheng, T. Wang, Z. Li, C. Guo, J. Lai and Z. Tian, *ACS Appl. Mater. Interfaces*, 2021, **13**, 51726–51735.
35 S. R. Choi, K. M. Kim and J. G. Kim, *J. Mol. Liq.*, 2022, **365**, 120104.
36 M. HosseinpourRokni, R. Naderi, M. Soleimani, A. R. Jannat, M. Pourfath and M. Saybani, *J. Ind. Eng. Chem.*, 2021, **102**, 327–342.
37 S. A. Mahdy, S. A. Abdel-Gawad, R. M. El-Sherif and I. M. Ghayad, *Ind. Eng. Chem. Res.*, 2023, **62**, 11784–11794.
38 O. Sanni, S. A. Iwarere and M. O. Daramola, *ACS Omega*, 2022, **7**, 40740–40749.
39 Y. Chen, Y. Liu, W. Du, Q. Li, H. Wang, Q. Li, Q. Wu and G. Qin, *J. Energy Storage*, 2024, **88**, 111397.
40 S. Choi, D. Lee, G. Kim, Y. Y. Lee, B. Kim, J. Moon and W. Shim, *Adv. Funct. Mater.*, 2017, **27**, 1702244.
41 T. Hu, K. Li, Y. Fang, L. Su, Z. Song, H. Shen and L. Sheng, *Int. J. Energy Res.*, 2019, **43**, 1099–1110.
42 J. Ryu, M. Park and J. Cho, *Adv. Mater.*, 2018, **31**, 1804784.
43 A. Pfrang, D. Veyret, F. Sieker and G. Tsotridis, *Int. J. Hydrogen Energy*, 2010, **35**, 3751–3757.
44 C. Lv, Y. Li, Y. Zhu, Y. Zhang, J. Kuang, D. Huang, Y. Tang and H. Wang, *Chem. Eng. J.*, 2023, **462**, 142182.
45 J. Ren, C. Fu, Q. Dong, M. Jiang, A. Dong, G. Zhu, J. Zhang and B. Sun, *ACS Sustainable Chem. Eng.*, 2021, **9**, 2300–2308.
46 J. Yang, D. Zhang, T. Lin, W. Zhang, C. Li and L. Gao, *J. Taiwan Inst. Chem. Eng.*, 2022, **131**, 104150.
47 P. K. Narayanam, P. Soni, V. D. Botcha, G. Singh and S. S. Major, *ACS Appl. Nano Mater.*, 2018, **1**, 5691–5701.
48 S. H. Hsiao, C. W. Chen and G. S. Liou, *J. Polym. Sci., Part A: Polym. Chem.*, 2004, **42**, 3302–3313.
49 F. Ridwan, D. Agusta, M. A. Husin and D. Dahlan, *Mater. Sci. Energy Technol.*, 2025, **8**, 24–31.
50 T. Huong Pham, W.-H. Lee and J.-G. Kim, *J. Mol. Liq.*, 2022, **347**, 118269.
51 H. Yang, X. Li, Y. Wang, L. Gao, J. Li, D. Zhang and T. Lin, *J. Power Sources*, 2020, **452**, 227785.
52 A.-L. Chen, N. Shang, Y. Ouyang, L. Mo, C. Zhou, W. W. Tjiu, F. Lai, Y.-E. Miao and T. Liu, *eScience*, 2022, **2**, 192–200.
53 W.-J. Long, X.-Q. Li, Y. Yu and C. He, *J. Mol. Liq.*, 2022, **360**, 119522.
54 C. Lv, Y. Zhu, Y. Li, Y. Zhang, J. Kuang, Y. Tang, H. Li and H. Wang, *Energy Storage Mater.*, 2023, **59**, 102756.
55 R. K. Harchegani and A. R. Riahi, *J. Electrochem. Soc.*, 2022, **169**, 030542.
56 C. Zhu, L. Yan, Y. Han, L. Luo, J. Guo, B. Xiang, Y. Zhou, X. Zou, L. Guo and Y. Bai, *Chem. Eng. J.*, 2024, **485**, 149600.
57 M. H. Shahini, M. Keramatinia, M. Ramezanzadeh, L. Guo and B. Ramezanzadeh, *J. Mol. Liq.*, 2022, **355**, 118950.
58 Y. Liu, Z. Gao, Z. Li, J. Zhang, Z. Qin, Y. Tang, Y. Xu, Z. Wu and W. Hu, *J. Energy Storage*, 2024, **88**, 111537.
59 M. A. Deyab and Q. Mohse, *J. Power Sources*, 2021, **506**, 230171.